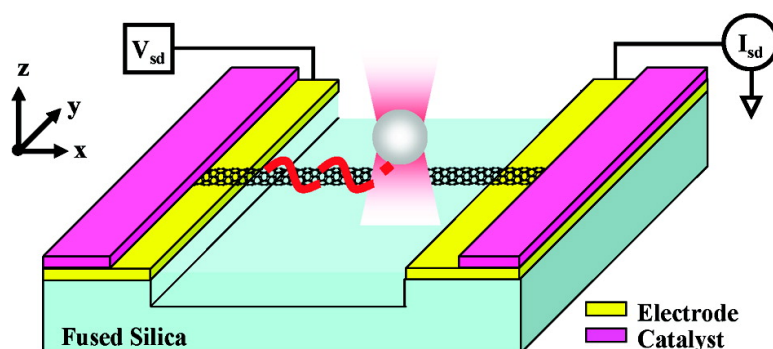


Bending and Twisting of Suspended Single-Walled Carbon Nanotubes in Solution

Ya-Qiong Xu, Arthur Barnard, and Paul L. McEuen

Nano Lett., Article ASAP • DOI: 10.1021/nl803861c • Publication Date (Web): 12 March 2009

Downloaded from <http://pubs.acs.org> on March 14, 2009



More About This Article

Additional resources and features associated with this article are available within the HTML version:

- Supporting Information
- Access to high resolution figures
- Links to articles and content related to this article
- Copyright permission to reproduce figures and/or text from this article

[View the Full Text HTML](#)

Bending and Twisting of Suspended Single-Walled Carbon Nanotubes in Solution

Ya-Qiong Xu,[†] Arthur Barnard,[‡] and Paul L. McEuen^{*†}

Laboratory of Atomic and Solid State Physics and School of Applied and Engineering Physics, Cornell University, Ithaca, New York 14850

Received December 22, 2008; Revised Manuscript Received February 25, 2009

ABSTRACT

We combine suspended carbon nanotube transistors with optical trapping techniques and scanning photocurrent microscopy to investigate the motion of suspended single-walled carbon nanotubes in solution. We study the movement of nanotubes by monitoring their photocurrent images and measure their thermal fluctuations by imaging microbeads that are tightly attached to nanotubes by single-stranded DNA. By analyzing their thermal fluctuations, we are able to obtain the torsional and bending stiffness of nanotubes and then calculate their diameters. We can also measure, with subangstrom resolution, the effective attachment point of the microbead to the nanotube.

Due to their small size, high electrical conductivity, unique mechanical properties, and low chemical reactivity,^{1–15} single-walled carbon nanotubes (SWNTs) have emerged as one of the most promising nanomaterials for biological and biomedical applications, such as biosensors, drug delivery, and imaging.^{16–28} However, applications are encumbered by the poor understanding of the behavior of nanotubes in solution and the lack of methods to directly manipulate nanotubes by molecular-scale forces. In this paper, we present the first measurement of the behavior of suspended nanotubes in solution by our new optoelectronic imaging system which combines optical trapping techniques^{29,30} with scanning photocurrent microscopy.^{31,32} We also use an optical trap to manipulate nanotubes by pulling on microbeads which are bound to nanotubes by single-stranded DNA (ssDNA). Finally, we show how to use this setup to measure the atomic motion of ssDNA on the sidewall of nanotubes.

We begin with a brief review of the expected properties of nanotubes in solution and the estimates of the sensitivity required to measure their behavior. Nanotubes are stiff linear polymers, which have been shown to follow continuum mechanics.^{9–13} Therefore, a nanotube can be treated as a cylinder fixed at both ends, whose transverse stiffness is

$$k_t = \frac{24\pi d^3 \Delta r E}{L^3}$$

For Young's modulus $E = 1$ TPa, a typical diameter $d = 2$ nm, wall thickness $\Delta r = 0.34$ nm, and length $L = 3$ μm ;

this yields $k_t \sim 10^{-2}$ pN/nm. Thermal fluctuation forces will cause movement on the nanometer scale

$$\Delta x = \sqrt{\frac{k_B T}{k_t}} \sim 20 \text{ nm}$$

with a characteristic time scale

$$t = \frac{\Delta x^2}{2D} \sim 0.2 \text{ ms}$$

where

$$D = \frac{k_B T \ln(L/d)}{4\pi\eta L} \approx 1 \mu\text{m}^2/\text{s}$$

with viscosity $\eta = 1$ mPa·s. Piconewton scale static forces will also cause movement; these can be applied using optical tweezers or drag from fluid flow

$$F_d = \frac{4\pi\eta L}{\ln(L/d)} v \sim 1 \text{ pN}$$

for 200 $\mu\text{m}/\text{s}$ flow rate. The challenge therefore is to measure nanometer-scale motion with millisecond-scale temporal resolution, in response to thermal fluctuations or piconewton-scale external forces.

Figure 1a shows a schematic diagram of the carbon nanotube transistors studied here. A 3 μm wide and deep trench was etched into a 170 μm thick fused silica double-side polished substrate by an Oxford PlasmaLab 80+ RIE system. The source and drain electrodes (2 nm Ti, 40 nm Pt) were separated by 7 μm . Catalyst pads (10 nm of Al_2O_3 , 0.2 nm of Fe) were deposited on the top of metal electrodes. SWNTs were then grown using a "fast heating" chemical vapor deposition method.³³ A 100 by 20 μm microfluidic poly(dimethylsiloxane) (PDMS) channel was sealed over the

* Corresponding author: tel, 607-255-4176; fax, 607-255-4176; e-mail, mceuen@ccmr.cornell.edu.

[†] Laboratory of Atomic and Solid State Physics.

[‡] School of Applied and Engineering Physics.

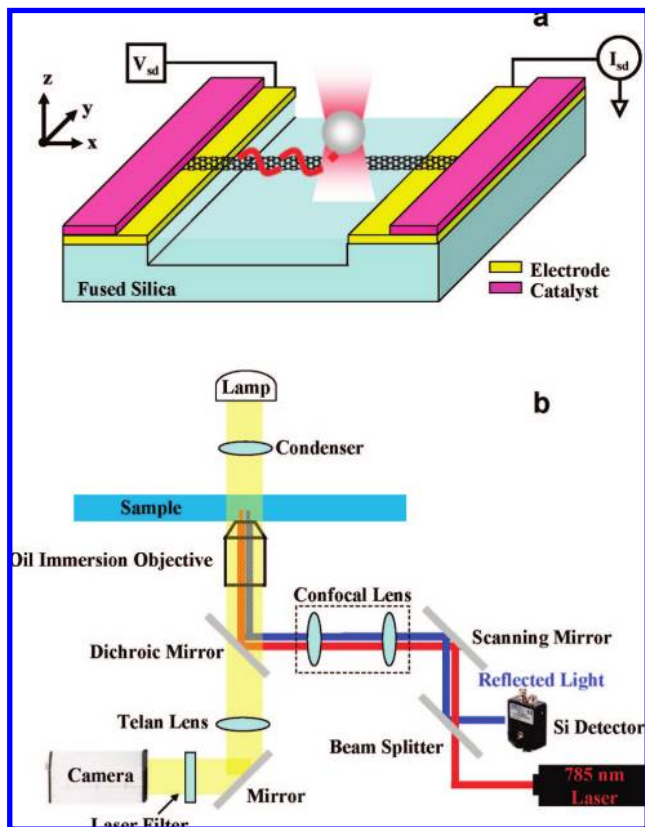


Figure 1. (a) Schematic description of an electrolyte-gated suspended nanotube transistor inside a PDMS microfluidic channel. (b) Schematic of the optoelectronic imaging system (not all components displayed). Light pathways are indicated for the halogen lamp (light yellow), trapping laser (red), and reflected light from the device (blue). Scanning mirrors move the trapping laser. Two confocal lenses expand the trapping laser beam. The dichroic mirror reflects trapping laser and transmits bright-field illumination. The Si photodetector collects the reflected light from the device. An optical filter isolates the bright-field illumination and blocks the trap laser.

SWNT, and a gold wire in a reservoir on the end of the channel was used to set the electrochemical potential of the solution. We can also attach a microbead to the nanotube using a ssDNA linker, as shown in Figure 1a. This bead can be easily visualized and manipulated using standard imaging/optical trapping techniques.

The optoelectronic imaging/optical trapping system is shown in Figure 1b. A single beam is formed by focusing a continuous-wave, near-infrared laser (80 mW, 785 nm) to a diffraction-limited spot of ~ 500 nm using an oil immersion $100\times$ Olympus microscope objective of high numerical aperture ($NA = 1.4$). The beam can be scanned over the sample with a piezo-controlled mirror with nanometer-scale spatial resolution. The scanned beam can be used both to perform photocurrent measurements and act as an optical tweezer, as discussed separately below.

We used a Sony XCD-V60 progressive scan CCD camera to automatically record the position of the microbead. Our approach for three-dimensional tracking of microbeads identifies the center in the focal plane, or xy plane from two-dimensional (2-D) bright-field video

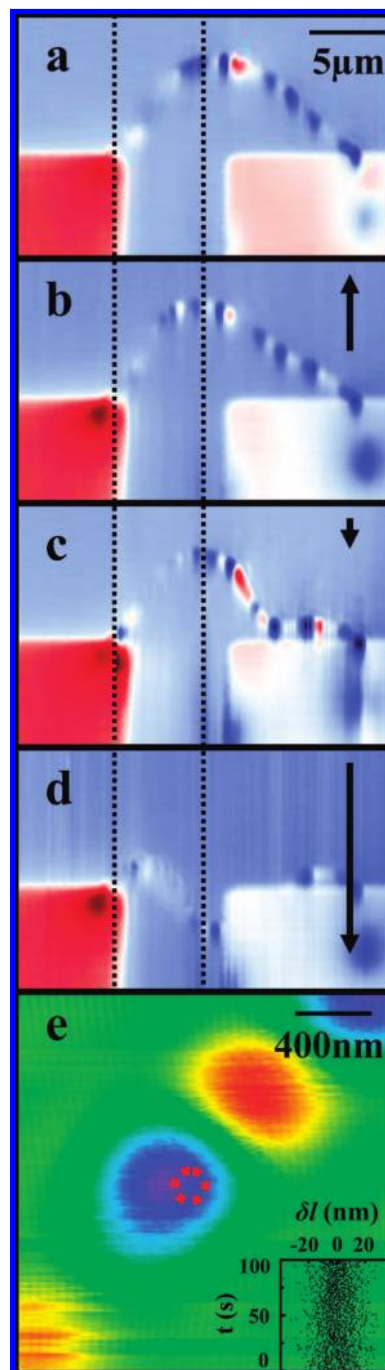


Figure 2. (a–d) Photocurrent images of a suspended nanotube transistor pulled by flow with different directions. The photocurrent response in nanoamperes is measured for a 5 mW laser. The metal contacts and the trench can also be seen in the reflected light signal, which is measured simultaneously with the photocurrent signal. By overlaying the reflected light image on the photocurrent response, we can locate the position of the nanotube relative to the contact edges. Large thermoelectric signals are seen at the two metal contacts, and a series of dots are seen along the nanotube. Here, photocurrent images are the photocurrent signal overlaid by the reflected light image. The black arrow represents the direction of fluid flow. The black dotted lines represent the edges of trenches: (a) no flow; (b) $100 \mu\text{m/s}$ upward; (c) $40 \mu\text{m/s}$ downward; and (d) $250 \mu\text{m/s}$ downward. (e) A photocurrent image of a nanotube. The inset is the spatial fluctuation when a laser is fixed to a place (red circle) close to a nanotube.

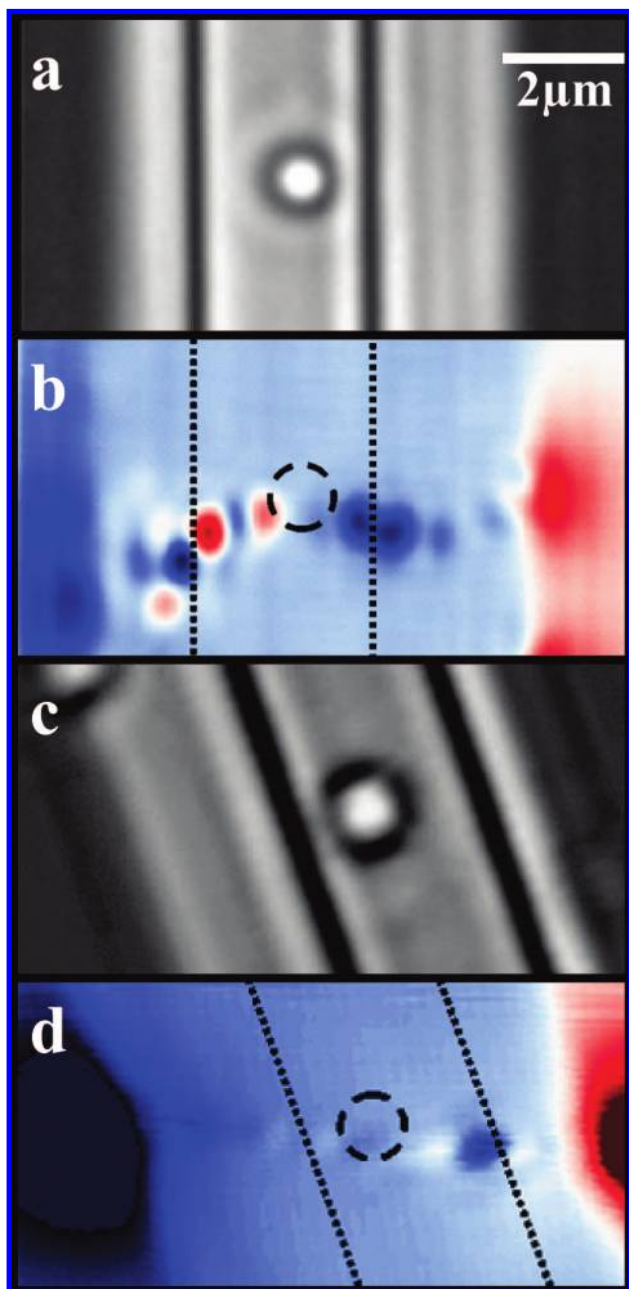


Figure 3. (a) An optical image and (b) photocurrent image of a microbead attached to a nanotube transistor by ssDNA. (c) and (d) Images for another transistor. The black circles in (b) and (d) represent microbeads.

microscope images using a well-known algorithm.³⁴ We then use out-of-focus optical effects to estimate the depth, or z -coordinate, of the microbead. We use a piezoelectric objective-lens position system (MIPOS 100) to calibrate the relation between the size and the brightness of the image with the z -coordinate. We then can locate the position of a $1 \mu\text{m}$ diameter microbead within 2 nm in the xy plane and 7 nm in the z -coordinate when the shutter speed of the CCD camera is 1 ms .

The first imaging technique uses the photocurrent response of a nanotube. When a diffraction-limited laser spot scans over the SWNT, a photocurrent signal occurs

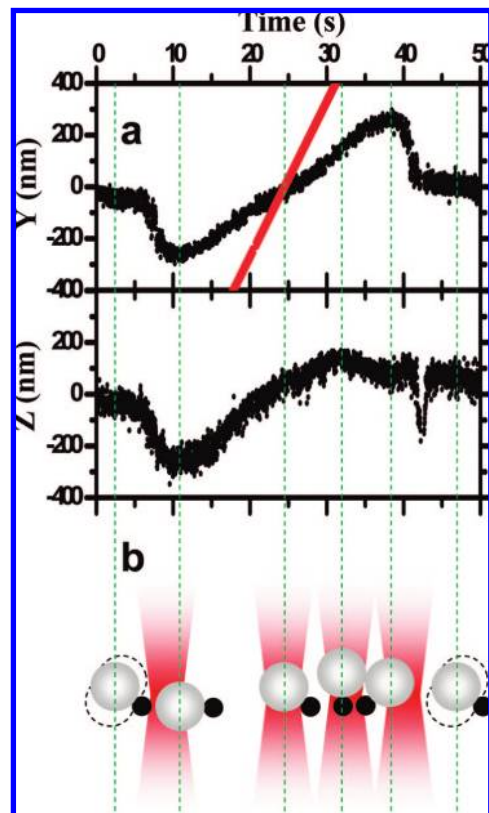


Figure 4. (a) The y and z position–time curve. (b) A schematic illustration of a microbead fixed to a nanotube and trapped by an optical tweezer.

Table 1. Experimental Measurement of Nanotubes' Moduli

device	k_t (pN/nm)	k_o (pN/nm)	k_t/k_o
1	0.02	0.002	10
2	0.02	0.002	10
3	0.06	0.003	20
4	0.04	0.002	20

wherever the SWNT electronic band structure bends: the built-in electrical field separates the photoexcited electron and hole and thus produces a current.^{31,32} This current is measured as a function of position, as shown in Figure 2, typically producing a series of spots along the nanotube, wherever disorder, contacts, or substrate interactions produce strong carrier separation. The center of the spots corresponds to a location of the nanotube, and this position can be measured with precision much greater than the diffraction limit. To determine the spatial and temporal resolution of this technique, we fix the laser on the edge of the spot and measure the fluctuation in the current, $\delta I = I(t + 50 \text{ ms}) - I(t)$. We convert this to a distance δl using the measured $\delta l/\delta I = 100 \text{ nm/nA}$ from the image. The root-mean-square of the spatial fluctuation is about 10 nm , as shown in the inset of Figure 2e.

To illustrate this technique, we image the ability of the surfactant sodium dodecylbenzene sulfonate (SDBS) to solubilize a nanotube initially attached to a surface. We injected deionized (DI) water in the reservoir and roughly controlled the flow direction by varying the relative sizes of the droplets in each reservoir.³⁵ The nanotube did not

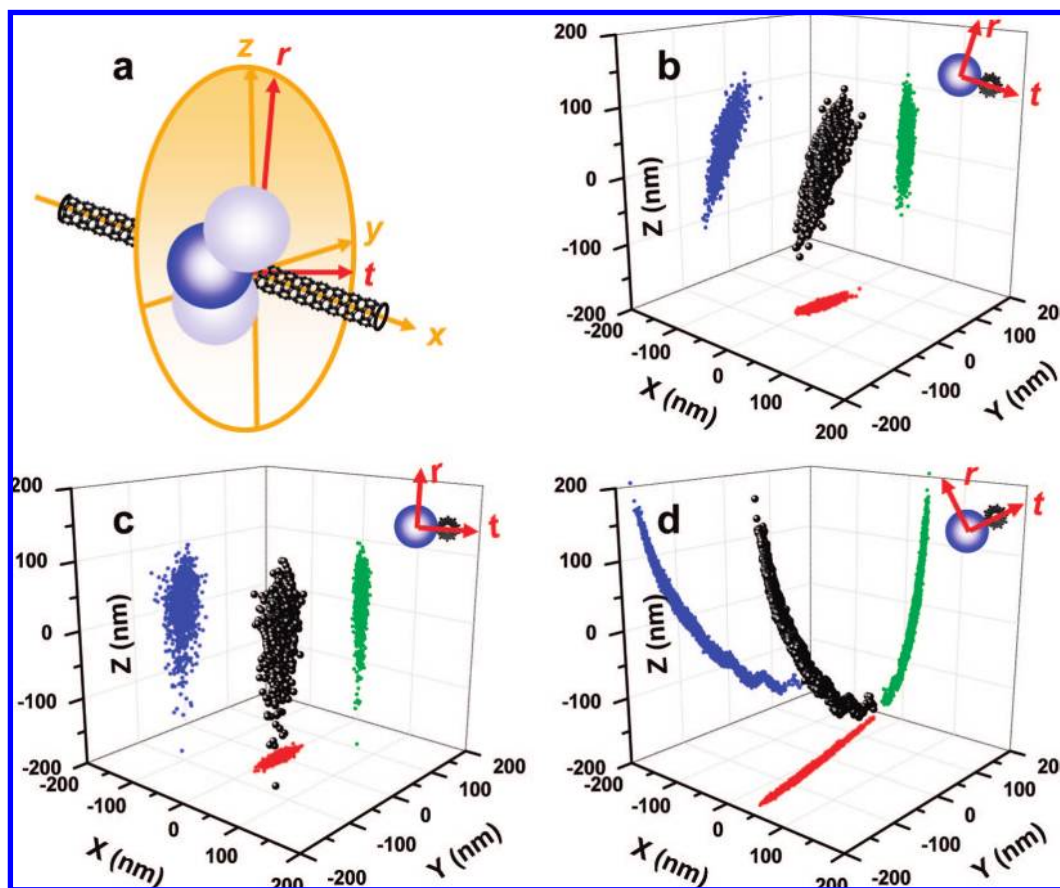


Figure 5. (a) A schematic description and (b–d) the three-dimensional view and projection of thermal fluctuations of a microbead attached to a nanotube by ssDNA for three different devices. The inset shows the transverse and torsional directions of each device.

move, indicating that it was stuck to the substrate. However, when we introduced 1 wt % SDBS surfactant in the reservoir, SDBS wrapped the nanotube and made it soluble in solution,³⁶ and the nanotube could easily be pulled by the flow, as shown in Figure 2. The natural shape of the nanotube was bowed away from the electrodes (Figure 2a). This shape can be reversed by a sufficiently large drag force 1.3 pN, corresponding to a flow rate of 250 $\mu\text{m/s}$ (Figure 2d).

To apply controlled forces and to more accurately measure the nanotube motion, we turn to measurements of nanotubes with microbeads attached. We injected 1X phosphate-buffered saline (PBS, pH 7.4) buffer solution together with 1 μm diameter microbeads into the reservoir. These microbeads were covalently attached to 50 kilobase pair ssDNA from calf thymus (Discovery Scientific Inc. PPS-1.0 DNA). When a microbead is near a nanotube, the ssDNA linked to this microbead will tightly wrap around the nanotube due to the aromatic interactions between nucleotide bases and nanotube sidewalls.^{18,37–41}

Figure 3 shows two suspended nanotube transistors with beads attached, along with photocurrent images of the nanotube, showing that the microbead is localized at the same position as the nanotube. (Movies of the attachment process are available in the Supporting Information.) Once attached, the microbeads can be manipulated with the optical tweezer to measure the mechanical response of the nanotube. The

optical trap was moved along the y axis shown as the red line in the top plot of Figure 4a. When the laser was far away from the nanotube, the microbead was unaffected. When the distance between the laser and the nanotube was only a few hundred nm, the microbead was caught by the optical trap. The microbead followed the trap as the laser was scanned near the nanotube. When the laser was moved further away, the microbead released and returned to its equilibrium position (Figure 4a). (The video related to the optical tweezer dragging the microbead is in the Supporting Information.)

Interestingly, the microbead moved along the z direction when the optical tweezer dragged it along the y direction, as shown in the bottom plot of Figure 4a. The schematic diagram in Figure 4b shows the movement of the microbead when the laser is in different positions. Evidently, the microbead rotates around the axis of the nanotube while the laser dragged it along the y direction. This suggests that rotation, not translation, is the dominant movement.

Measurements of the thermal fluctuations of the microbeads confirm this picture. Figure 5 outlines the three-dimensional view and projections of thermal fluctuations of microbeads attached to nanotubes. (Videos are included in the Supporting Information.) The fluctuations in the position of the microbeads are highly anisotropic. First, they are comparable to the instrument resolution along the length, indicating that the microbead does not move along the length

of the tube. In the plane perpendicular to the tube, the fluctuations are elongated along a direction that is different for each device.

The origin of this behavior is clear from the device in Figure 5d. The fluctuations are along an arc, and the radius of this arc is $0.5 \mu\text{m}$, the radius of the microbead. This motion, therefore, corresponds to fluctuations in which the microbead rotates around the axis of the nanotube, as shown in Figure 5a. The attachment point of the microbead to the nanotube determines the orientation of the fluctuations, as shown in the insets to the figure.

By analyzing the thermal fluctuations of the microbead position, we can use the equipartition theorem to calculate the transverse stiffness

$$k_t = \frac{k_B T}{\Delta x^2}$$

and torsional stiffness

$$\kappa_\theta = \frac{k_B T}{\Delta \theta^2}$$

of the nanotube spring. The measured data are position displacements (Δx) instead of angular displacements ($\Delta \theta$), so we define the effective torsional stiffness as $k_\theta \equiv \kappa_\theta / R^2$, where $R = 0.5 \mu\text{m}$ is the radius of the microbead. Here the microbead acts as a long lever arm; therefore, the size of the rotational thermal fluctuation of a nanotube is amplified hundreds of times. Since we can locate the position of a microbead with 10 nm resolution, we are able to observe the motion of a nanotube with subangstrom resolution.

Table 1 shows the calculated stiffness for four different devices. The transverse stiffnesses of these devices are $\sim 0.02\text{--}0.06$ pN/nm and the effective torsional stiffnesses of these devices are $0.002\text{--}0.003$ pN/nm, respectively. In general, the nanotube's effective torsional stiffness is about 10–20 times smaller than its transverse stiffness.

On the basis of the continuum mechanics model, the effective torsional stiffness can be estimated if a rigid, fixed attachment between the microbead and the nanotube is assumed

$$k_\theta = \frac{\kappa_\theta}{R^2} \approx \frac{\pi d^3 \Delta r G}{4LR^2}$$

where $G = 330$ GPa is shear modulus and $L = 3 \mu\text{m}$ is the length of the suspended section of the nanotube. The ratio of the nanotube's transverse to its effective torsional stiffness is

$$\frac{k_t}{k_\theta} = \frac{96R^2 E}{L^2 G} \approx 8$$

independent of the diameter of the nanotube. This is in good agreement with the results of Table 1, indicating that both the transverse and torsional stiffnesses observed represent the properties of the nanotube and not the microbead/linker. The diameters estimated from both the transverse and effective torsional stiffness are about 3 nm for all four devices, which is typical for the growth method used. Unfortunately, the rough fused silica substrate and suspended geometry prohibit accurate confirmation of these values by atomic force microscopy.

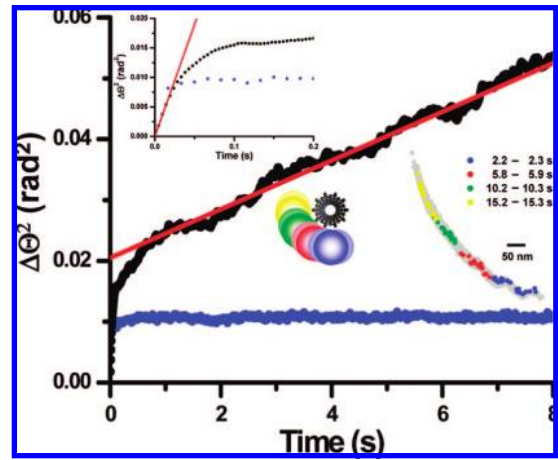


Figure 6. The mean square angle displacement along the rotational direction of the thermal fluctuations of a nanotube. The black and blue dots are the experiment data for two different devices. The red line has a slope of $0.004 \text{ rad}^2/\text{s}$. The upper left inset is zoom-in of the short time scale, where the red line has a slope of $0.4 \text{ rad}^2/\text{s}$. In the lower right inset, the gray dots represent the fluctuation of the nanotube in the entire 30 s time span. Four different colors dots represent four separate 100 ms scale fluctuations. The lower left inset is the schematic description of this motion.

We can also calculate the roll-off time of the rotational fluctuations using the angular autocorrelation function. If the attachment of the microbead to the nanotube is rigid and unmoving, the mean square angle displacement

$$\Delta \Theta^2(\tau) = \frac{1}{N} \sum_{i=1}^N (\Theta(t_i + \tau) - \Theta(t_i))^2$$

should initially grow linearly with time and then approach a constant. The upper left inset of Figure 6 shows this initial rise, with a characteristic time of about 100 ms. From this linear region, we can determine the nanotube/microbead system's rotational diffusion constant, which is

$$D = \frac{\Delta \Theta^2(\tau)}{2\tau} = 0.2 \text{ rad}^2/\text{s}$$

This has the same order as a theoretical estimate based on the contribution from both the rotational diffusion of a 3 nm diameter nanotube and the translation diffusion of a $1 \mu\text{m}$ diameter microbead attached to the nanotube.

For long times, $\Delta \Theta^2(\tau)$ of most devices approaches a constant value, as shown in the blue dotted line in Figure 6 and as theoretically expected. This is typically the case, but not always, such as the device shown in the black dotted line (Figure 6). After the initial rise associated with thermal diffusion of the nanotube/microbead system, we see a second slow rise. The diffusion constant for the slow process is $0.002 \text{ rad}^2/\text{s}$, which is about 100 times smaller than the nanotube's diffusion constant in solution. The origin of this slow diffusion is illustrated in the lower insets of Figure 6. In 100 ms, the microbead fluctuates around an equilibrium position. However, at a later time, this equilibrium position is different. This indicates that the attachment point is not fixed but rather diffuses along the surface of the nanotube.

We can easily track changes in the attachment point on the atomic scale. Assuming a 3 nm diameter nanotube, the

length of the carbon–carbon bond (0.14 nm) corresponds to an angular change of 0.1 rad, or a movement of the microbead by 50 nm, the size of the scale bar in the right inset of Figure 6. This approach thus provides a platform to detect the atomic motion of ssDNA or other molecules attached to the sidewall of nanotubes. Furthermore, electrical or thermal signals can be applied to influence the motion of biomolecules, as well as the rate of biological reactions. This should be invaluable in providing quantitative information about molecular binding to nanotubes.

In conclusion, we have developed a high spatial and time resolution optoelectronic imaging system to measure and manipulate the motion of suspended carbon nanotubes. We obtain the torsional and transverse moduli of the nanotubes from measuring their thermal fluctuations. This system provides a new way to measure the diameters of suspended nanotubes in solution and the atomic motion of ssDNA on the sidewall of nanotubes. These experiments not only extend the understanding of the mechanical properties of nanotubes in solution but also provide a framework to investigate the interactions between nanotubes and biological molecules.

Acknowledgment. The authors thank Professor Michelle Wang's and Professor Itai Cohen's groups for the help and discussion. The authors also thank the Nanobiotechnology Center, a STC Program of the National Science Foundation under Agreement No. ESC-9876771, for support of this research, and the authors are grateful for a gift from the Agilent Technologies Foundation.

Supporting Information Available: Videos of the attachment, drag, and fluctuation of microbeads to nanotubes by ssDNA. This material is available free of charge via the Internet at <http://pubs.acs.org>.

References

- McEuen, P. L.; Park, J. *Mater. Res. Soc. Bull.* **2004**, *29*, 272.
- Walters, D. A.; Ericson, L. M.; Casavant, M. J.; Liu, J.; Colbert, D. T.; Smith, K. A.; Smalley, R. E. *Appl. Phys. Lett.* **1999**, *74*, 3803.
- Yu, M. F.; Louries, O.; Dyer, M. J.; Moloni, K.; Kelly, T. F.; Ruoff, R. S. *Science* **2000**, *287*, 637.
- Salvetat, J. P.; Bonard, J. M.; Thomson, N. H.; Kulik, A. J.; Forro, L.; Benoit, W.; Zuppiroli, L. *Appl. Phys. A: Mater. Sci. Process.* **1999**, *69*, 255.
- Wong, E. W.; Sheehan, P. E.; Lieber, C. M. *Science* **1997**, *277*, 1971.
- Tombler, T. W.; Zhou, C. W.; Alexseyev, L.; Kong, J.; Dai, H.; Liu, L.; Jayanthi, C. S.; Tang, M.; Wu, S. Y. *Nature* **2000**, *405*, 769.
- Huang, M.; Wu, Y.; Chandra, B.; Yan, H.; Shan, Y.; Heinz, T. F.; Hone, J. *Phys. Rev. Lett.* **2008**, *100*, 136803.
- Minot, E. D.; Yaish, Y.; Sazonova, V.; Park, J. Y.; Brink, M.; McEuen, P. L. *Phys. Rev. Lett.* **2003**, *90*, 156401.
- Hall, A. R.; Falvo, M. R.; Superfine, R.; Washburn, S. *Nat. Nanotechnol.* **2007**, *2*, 413.
- Hall, A. R.; An, L.; Vicci, L.; Falvo, M. R.; Superfine, R.; Washburn, S. *Phys. Rev. Lett.* **2006**, *96*, 256102.
- Salvetat, J. P.; Briggs, A. D.; Bonard, J. M.; Bacsá, R. R.; Kulik, A. J.; Stöckli, T.; Burnham, N. A.; Forró, L. *Phys. Rev. Lett.* **1999**, *82*, 944.
- Wong, E. W.; Sheehan, P. E.; Lieber, C. M. *Science* **1997**, *277*, 1971.
- Treacy, M. M. J.; Ebbesen, T. W.; Gibson, J. M. *Nature* **1996**, *381*, 678.
- Wu, Z.; Chen, Z.; Du, X.; Logan, J. M.; Sippel, J.; Nikolou, M.; Kamaras, K.; Reynolds, J. R.; Tanner, D. B.; Hebard, A. F.; Rinzler, A. G. *Science* **2004**, *305*, 1273.
- Purewal, M. S.; Hong, B. H.; Ravi, A.; Chandra, B.; Hone, J.; Kim, P. *Phys. Rev. Lett.* **2007**, *98*, 186808.
- Goldsmith, B. R.; Coroneus, J. G.; Khalap, V. R.; Kane, A. A.; Weiss, G. A.; Collins, P. G. *Science* **2007**, *315*, 77.
- Kong, J.; Franklin, N. R.; Zhou, C.; Chapline, M. G.; Peng, S.; Cho, K.; Dai, H. *Science* **2000**, *287*, 22.
- Star, A.; Tu, E.; Niemann, J.; Gabriel, J.; Joiner, C. S.; Valcke, C. *Proc. Natl. Acad. Sci. U.S.A.* **2006**, *103*, 92.
- Zhou, X. J.; Moran-Mirabal, J. M.; Craighead, H. G.; McEuen, P. L. *Nature Nanotech.* **2007**, *2*, 185.
- Wu, Y.; Phillips, J. A.; Liu, H.; Yang, R.; Tan, W. *ACS Nano* **2008**, *2*, 2023.
- Ko, S.; Liu, H.; Chen, Y.; Mao, C. *Biomacromolecules* **2008**, *9*, 3039.
- Liu, Z.; Li, X.; Tabakman, S. M.; Jiang, K.; Fan, S.; Dai, H. *J. Am. Chem. Soc.* **2008**, *130*, 13540.
- Zerda, A.; Zavaleta, C.; Keren, S.; Vaithilingam, S.; Bodapati, S.; Liu, Z.; Levi, J.; Smith, B. R.; Ma, T. J.; Oralkan, O.; Cheng, Z.; Chen, X.; Dai, H. *Nat. Nanotechnol.* **2008**, *3*, 556.
- Liu, Z.; Chen, K.; Davis, C.; Sherlock, S.; Cao, Q.; Chen, X.; Dai, H. *Cancer Res.* **2008**, *68*, 6652.
- Welscher, K.; Liu, Z.; Daranciang, D.; Dai, H. *Nano Lett.* **2008**, *8*, 586.
- Kam, N. V.; Liu, Z.; Dai, H. *J. Am. Chem. Soc.* **2005**, *127*, 12492.
- Kam, N. V.; O'Connell, M.; Wisdom, J. A.; Dai, H. *Proc. Natl. Acad. Sci. U.S.A.* **2005**, *102*, 11600.
- Kam, N. V.; Liu, Z.; Dai, H. *Angew. Chem., Int. Ed.* **2006**, *45*, 577.
- Ashkin, A.; Dziedzic, J. M. *Science* **1987**, *235*, 1517.
- Neuman, K. C.; Block, S. M. *Rev. Sci. Instrum.* **2004**, *75*, 2787.
- Avouris, P.; Chen, Z. H.; Perebeinos, V. *Nat. Nanotechnol.* **2007**, *2*, 605.
- Ahn, Y.; Dunning, J.; Park, J. *Nano Lett.* **2005**, *5*, 1367.
- Huang, S.; Cai, X.; Liu, J. *J. Am. Chem. Soc.* **2003**, *125*, 5636.
- Crocker, J.; Grier, D. G. *J. Colloid Interface Sci.* **1996**, *179*, 298.
- Hirsa, A. H.; Lopez, C. A.; Laytin, M. A.; Vogel, M. J.; Steen, P. H. *Appl. Phys. Lett.* **2005**, *86*, 014106.
- O'Connell, M. J.; Bachilo, S. M.; Huffman, C. B.; Moore, V. C.; Strano, M. S.; Haroz, E. H.; Rialon, K. L.; Boul, P. J.; Noon, W. H.; Kittrell, C.; Ma, J.; Hauge, R. H.; Weisman, R. B.; Smalley, R. E. *Science* **2002**, *297*, 593.
- Zheng, M.; Jagota, A.; Semke, E. D.; Diner, B. A.; Mclean, R. S.; Lustig, S. R.; Richardson, R. E.; Tassi, N. G. *Nat. Mater.* **2003**, *2*, 338.
- Johnson, R. R.; Johnson, T. C.; Klein, M. L. *Nano Lett.* **2008**, *8*, 69.
- Manohar, S.; Tang, T.; Jagota, A. *J. Phys. Chem. C* **2007**, *111*, 17835.
- Cathcart, H.; Nicolosi, V.; Hughes, J. M.; Blau, W. J.; Kelly, J. M.; Quinn, S. J.; Coleman, J. N. *J. Am. Chem. Soc.* **2008**, *130*, 12734.
- Gigliotti, B.; Sakizze, B.; Bethune, D. S.; Shelby, R. M.; Cha, J. N. *Nano Lett.* **2006**, *6*, 159.

NL803861C